Author Manuscript

Author Manuscript

Author Manuscript

Author Manuscript

HHS Public Access

Author manuscript

Nat Protoc. Author manuscript; available in PMC 2020 December 15.

Published in final edited form as:

Nat Protoc. ; 6(10): 1536–1545. doi:10.1038/nprot.2011.385.

3D maps of RNA interhelical junctions

Maximillian H Bailor[1,2], **Anthony M Mustoe**[1,2], **Charles L Brooks III**[1], **Hashim M Al-Hashimi**[1]

[1]Department of Chemistry and Biophysics, The University of Michigan, Ann Arbor, Michigan, USA.

Abstract

More than 50% of RNA secondary structure is estimated to be A-form helices, which are linked together by various junctions. Here we describe a protocol for computing three interhelical Euler angles describing the relative orientation of helices across RNA junctions. 5′ and 3′ helices, H1 and H2, respectively, are assigned based on the junction topology. a reference canonical helix is constructed using an appropriate molecular builder software consisting of two continuous idealized A-form helices (iH1 and iH2) with helix axis oriented along the molecular *Z*-direction running toward the positive direction from iH1 to iH2. the phosphate groups and the carbon and oxygen atoms of the sugars are used to superimpose helix H1 of a target interhelical junction onto the corresponding iH1 of the reference helix. A copy of iH2 is then superimposed onto the resulting H2 helix to generate iH2′. A rotation matrix *R* is computed, which rotates iH2′ into iH2 and expresses the rotation parameters in terms of three Euler angles α_h, β_h and γ_h. The angles are processed to resolve a twofold degeneracy and to select an overall rotation around the axis of the reference helix. The three interhelical Euler angles define clockwise rotations around the 5′ ($-\gamma_h$) and 3′ (α_h) helices and an interhelical bend angle (β_h). The angles can be depicted graphically to provide a ‘Ramachandran’-type view of RNA global structure that can be used to identify unusual conformations as well as to understand variations due to changes in sequence, junction topology and other parameters.

INTRODUCTION

Geometric descriptors of conformation are indispensable for analyzing the complex structures of biomolecules. For example, the description of polypeptide backbones in terms of ϕ and ψ torsion angles and their visualization using Ramachandran maps have become the common ways to analyze protein structure, have helped to uncover many of the guiding principles of protein architecture and they are now routinely used to assess newly determined protein structures[1–6]. Local descriptors of nucleic acid structure, including

Reprints and permissions information is available online at http://www.nature.com/reprints/index.html.

correspondence should be addressed to H.M.A.-H. (hashimi@umich.edu).

AUTHOR CONTRIBUTIONS All authors contributed to the work presented in this paper. M.H.B. and H.M.A.-H. conceived the original protocol, developed the underlying theory and performed the analysis. A.M.M. developed theory and performed analysis to define the various Euler angle conventions, improve the robustness of the protocol and establish its limits of applicability. C.L.B. performed supporting simulations to assess the robustness of the protocol. M.H.B., A.M.M., C.L.B. and H.M.A.-H. prepared the manuscript.

[2]These authors contributed equally to this work.

COMPETING FINANCIAL INTERESTS The authors declare no competing financial interests.

Author Manuscript Author Manuscript Author Manuscript Author Manuscript

helical and base pair parameters as well as sugar and phosphodiester torsions and other parameterizations thereof, have also been invaluable in the analysis of RNA and DNA structures[7–10]. At much larger length scales, radius of gyration and the distance distribution function, $P(r)$, provide a coarse description of global conformation, which can be measured relatively easily using a variety of biophysical techniques without the need for high-resolution structure determination[11–14].

For both proteins and nucleic acids, there exists a gap between atomic-level descriptors of local structure and the much coarser description of global shape. A natural link between these two scales is the relative orientation and translation of secondary structure building block elements. More than 50% of RNA secondary structure is estimated to be A-form helices[15], which are linked together by various junctions, including internal loops, bulges and high-order junctions[16–18]. To a very large extent, RNA's global shape is defined by the relative orientation of A-form helices. Moreover, surveys of the growing database of RNA structures reveal that the A-form helix assumes a similar local conformation in a variety of contexts[19]. This makes it possible to use an idealized A-form helix geometry to approximate helical stems in RNA. In other words, unlike secondary structural elements in proteins that can have sequence-specific variations in shape, the A-form helix reoccurs in similar form, making it a fundamental building block of RNA global structure.

A standardized approach for describing the orientation (and translation) of RNA A-form helices can bridge the divide between atomic- and coarser-level descriptions of structure, providing a Ramachandran-type view of RNA global structure that can be used to identify unusual conformations, as well as to understand variations due to changes in sequence, junction topology and other parameters of interest. Because helices are chiral objects, three angles are required to specify the orientation of one helix relative to another. Traditionally, studies have focused on the interhelical bend angle, which proves easier to measure/estimate without having to determine a high-resolution structure[20–35]. The advent of weak alignment NMR and the measurement of residual dipolar couplings in partially aligned RNA molecules[36–38] provided a route for determining two, and, in favorable cases, all three interhelical angles without the need for determining a high-resolution structure[30,32,39–41]. This spurred the development and standardization of three interhelical angles (α_h, β_h and γ_h) that can be used to describe the orientation of helices across any junction; α_h and γ_h specify a twist around the axis of each of the two helices and β_h specifies an interhelical bend angle (Fig. 1). Computation of these interhelical angles comprehensively for all RNA helices linked by two-way junctions in the protein data bank (PDB) led to the discovery of fundamental principles of junction architecture[10,42]. In analogy to Ramachandran plots, these studies revealed that simple steric and connectivity constraints (collectively referred to as topological constraints) severely restrict the allowed interhelical orientations to a small fraction (~10%) of the total (α_h, β_h, γ_h) space and that the space sampled can be programmatically varied by changing the junction topology[10,42].

Here we describe a protocol for computing, mapping and analyzing interhelical angles α_h, β_h and γ_h. The procedure can be used to compute angles for any structural model that shows the 3D orientation of helices. Although we focus on the description of angles across two-

Author Manuscript Author Manuscript Author Manuscript Author Manuscript

way junctions, this basic framework can be extended to describe all *N*-1 sets of angles needed to describe the orientation of *N* helices linked by an *N*-way junction.

Design: definitions and nomenclature

Idealized A-form helices as building block elements of RNA interhelical structure.

Surveys of X-ray and NMR structures of A-form helices in the PDB show that Watson-Crick (WC) base pairs that are surrounded by other WC base pairs adopt local conformations that to a very good approximation can be modeled as a canonical A-form helix[8,19,43]. The observed variations in base pair and base-pair step parameters across high-resolution X-ray structures are comparable to the variations in structure expected due to thermal motions[44–46]. This makes it possible to use the canonical A-form helix as a common building block for computing interhelical angles. In this protocol, idealized A-form helices are superimposed onto helices of interest in an RNA target, and their relative orientation defined relative to a common reference frame[42] (Fig. 2). WC base pairs adjacent to junctions and ends of helices are known to contain more structural noise and should be excluded from superposition of helices. For the most accurate results, a root-mean-square deviation (RMSD) superposition should be <2 Å or the computed interhelical angles will be unreliable. In general, an RMSD < 2 Å will yield α_h, β_h and γ_h errors on the order of ~5°.

Reference frame.

The establishment of a universal frame of reference is often key in the development and standardization of geometric descriptor of structure[7]. In our protocol, the orientation of two helices, H1 and H2, in a given junction, is defined relative to a reference helix in which the two helices are perfectly coaxially stacked[42] (Fig. 2). We choose a frame in which our idealized reference helix, containing helices iH1 and iH2, is aligned with helix axis oriented along the positive *Z*-direction from iH1 to iH2 (Fig. 1). This reference frame allows us to define the interhelical orientation in terms of three Euler angles (see below), which conveniently specifies rotations around each of the two helical axes and a direction normal to the helical axes[42] (Fig. 2). These interhelical Euler angles provide an intuitive geometric description of interhelical orientation that captures the pseudo-cylindrical symmetry properties of A-form helices[42].

Two-way junctions.

Two-way junctions consist of two helical stems that are adjoined by one or two strands containing noncanonical residues, such as lone nucleotide(s) and/or non-WC base pair(s). In this protocol, we consider a ‘helix’ to be three or more consecutive WC base pairs and two-way junctions to be non-WC base pairs that adjoin two helices. Note that with this definition, G-U base pairs, which occur frequently in RNA, would be considered to be junction residues if they are separated by two sufficiently long WC helices. However, in practice, a G-U base pair or other noncanonical base pair could be considered as a part of a helix if its backbone conforms to the idealized A-form geometry.

Author Manuscript Author Manuscript Author Manuscript Author Manuscript

Strand and helix assignments.

In two-way junctions, helices, H, are linked by one or two strands, S. The longer 'X' and shorter 'Y' strand contain *X* and *Y* residues, respectively ($X \geq Y$; Fig. 1). We define a reference helix, H1, as the helix that is linked to the 5′ end of the *X* strand (Fig. 1). Helix H2 is linked to the 3′ end of the *X* strand. Building on a previous convention by Lilley and co-workers[47], we designate two-way junctions using the 'bar code' $H_i S_X H_j . S_Y$, in which *i* and *j* specify the length (number of base pairs) of the 5′ and 3′ helices, respectively (Fig. 1a). The reference H1 helix can be assigned unambiguously except for symmetrical internal loops ($X = Y$). Here the reference helix is assigned arbitrarily, though one could also use other criteria to make a unique assignment, such as the sequence of closing base pairs. Note that the improper assignment of helices will result in the calculation of alternate interhelical Euler angles, α_h, β_h and γ_h, given by equation (1) (Table 1) where $\alpha_F(T_h°)$ is obtained from the rotation that superimposes helix iH1 onto iH2 and is dependent on the overall twist angle $T_h°$ (defined below).

Design: interhelical Euler angles

Definition of Euler angles.

In this protocol, the interhelical angles are computed by determining the rotation matrix $R(\alpha_h \beta_h \gamma_h)$ that transforms H2′ in a given target junction to an orientation that is coaxial with H1 (Fig. 2)[42]. We work in our reference frame, in which two idealized helices (iH1 and iH2) are perfectly coaxially stacked and oriented along the positive *Z*-direction from iH1 to iH2 (Fig. 2)[42]. An overall twist angle $T_h°$ defines a rotation around the reference helix axis (Fig. 2). We define $T_h°$ as the rotation angle about the helix axis between the closing-junction base pair *y* axis of iH1, as defined by Westhof and co-workers[48], projected onto the *x*-*y* plane of the molecular frame, and the *y* axis of the molecular frame. A common $T_h°$ angle has to be used when comparing interhelical angles for a set of junctions. Changing the value of $T_h°$ results in a uniform shift in Euler angles ($\alpha_h \pm T_h°$, $\beta_h = 0°$ or 180°, $\gamma_h \mp T_h°$). We do not specify a single $T_h°$ value, as in practice the value that minimizes the spread of orientations for a given distribution is selected (see below).

In our protocol, we determine $R(\alpha_h \beta_h \gamma_h)$ by first superimposing sugar and backbone atoms of H1 in a target junction onto iH1 of the reference helix (Fig. 2)[42]. Next, we superimpose a copy of iH2 onto the resulting H2 to generate iH2′ (Fig. 2)[42]. *R* is then computed from the coordinates of iH2′ and iH2 and parameterized in terms of Euler angles α_h, β_h and γ_h (Fig. 3)[42]. The parameterization of the rotation matrix in terms of Euler angles can be a great source of confusion and it is therefore important that we rigorously define our specific convention. We compute *R* and deduce (α_h, β_h, γ_h) directly from the rotation matrix, equation (2) (Table 1).

This Euler rotation is implemented in the program EULER-RNA (http://hashimi.biop.lsa.umich.edu/index.php?q=node/6)[41] and uses the *ZYZ* convention. Note that use of the *ZXZ* or other conventions leads to conceptually analogous but different angles. The above rotation matrix and the angles α_h, β_h and γ_h can be defined in several different yet equivalent ways (Fig. 3). In the 'local axis' definition, *R* rotates the object (i.e., the helix)

Author Manuscript Author Manuscript Author Manuscript Author Manuscript

through a succession of Euler rotations α_h, β_h and γ_h around the local axes Z, $\dot{Y}$ and $\dot{Z}$, respectively, from H2′ to H2 (Fig. 3a). Here positive angles correspond to anticlockwise rotation of the object (i.e., helix). The same transformation from H2′ to H2 can be viewed as rotation of the frame through a succession of α_h, β_h and γ_h Euler rotations around Z, $\dot{Y}$ and $\dot{Z}$ (Fig. 3b). Here positive angles correspond to clockwise rotation of the frame. Finally, in the 'global axis' definition, the rotations are applied to the object in the reverse order γ_h, β_h and α_h about the fixed global frame axes of Z, Y and Z, respectively[49] (Fig. 3c). Here positive angles correspond to anticlockwise rotation of the object.

It proves useful to consider the inverse rotation, R^{-1}, that transforms the helix from the reference frame (H2) to a given orientation (H2′; Fig. 3d). This can help better conceptualize the angles α_h, β_h and γ_h, as well as allow generation of a given junction with specified α_h, β_h and γ_h interhelical angles starting from the reference helix. The inverse rotation is given by:

$$R^{-1}(\alpha_h\beta_h\gamma_h) = R(-\gamma_h - \beta_h - \alpha_h)$$

Here $-\gamma_h$, $-\beta_h$ and $-\alpha_h$ correspond to anticlockwise rotations of the helix or equivalently, the angles γ_h, β_h and α_h denote clockwise rotations of the helix from H2 to H2′. As defined, all rotations are applied to H2. However, it is convenient to view the angle γ_h as rotation of H1 around its own axis by an angle $-\gamma_h$ (the minus sign is introduced here, as the relative interhelical orientation obtained by rotation of H2 in a coaxial helix by γ_h is equivalent to that obtained when rotating H1 by $-\gamma_h$). In this manner, the angles $-\gamma_h$ and α_h denote clockwise rotations of H1 and H2 about their respective helical axes.

An interhelical twist angle (ζ) can be defined $\zeta = \alpha_h + \gamma_h$ in which over- and under-twisting of the two helices correspond to negative and positive ζ values, respectively[42]. In principle, the twist angle between two helices can assume any arbitrary value. For example, a helix could be over-twisted by a quarter turn, a full turn or multiple turns. Note that in the absence of other information, $-180° \leq \zeta \leq 180°$, as for $\zeta \geq 180°$ and $\zeta \leq -180°$, it is impossible to distinguish between over-twisting by ζ versus undertwisting by $360° - \zeta$ and likewise between ζ and $\zeta + n \times \pm 360°$, where n is an integer. Also note that both the interhelical bend and twist angles are independent of $T_h°$.

Euler degeneracy.

The interhelical Euler angles (α_h, β_h, γ_h) are two old degenerate when limiting α_h β_h γ_h to ± 180°. A second solution is obtained because a given set of Euler angles α_h β_h γ_h are degenerate with respect to $\alpha_h \pm 180°$, $-\beta_h$, $\gamma_h \pm 180°$ and $\alpha_h \pm 180°$, $-\beta_h$, $\gamma_h \mp 180°$. For the special case of having perfectly parallel or antiparallel helices, there is a continuous coaxial degeneracy defined by ($\alpha_h \pm D$, $\beta_h = 0°$ or 180°, $\gamma_h \mp D$), where D is a constant. In our protocol, we lift this degeneracy by choosing the angles that minimize $\delta = \sqrt{\alpha_h^2 + \beta_h^2 + \gamma_h^2}$ (ref. 42). The latter serves to bias solutions to the pole (0, 0, 0), thus resulting in a compact distribution of Euler angles. Solutions can also be limited to values of β between 0° and 180°. Note, however, that this can lead to multimodal distributions that can complicate analysis of how the three angles covary with one another. For example, the two closely

Author Manuscript Author Manuscript Author Manuscript Author Manuscript

related orientations (45°, 10°, 45°) and (45°, −10°, 45°) would be represented as (45°, 10°, 45°) and (−135°, 10°, −135°), resulting in large disparities between the α_h and γ_h and appearance of two apparent ‘populations’ when plotted in the 3D maps.

Design: mapping and interpreting interhelical Euler angles

Following selection of one among two degenerate interhelical Euler angles, the three angles (α_h, β_h, $-\gamma_h$) for a set of junctions can be plotted in a single 3D cube (Fig. 4a) or alternatively, as a set of 3 × 2D plots (Fig. 4b). These types of plots make it possible to directly visualize how the three angles covary with one another. The interpretation of these maps must, however, take into account the intricacies and often nonintuitive aspects of the Euler space. In particular, the distance between any two junctions, n and m, in Euler space (i.e., $\sqrt{(\alpha_n-\alpha_m)^2+(\beta_n-\beta_m)^2+(\gamma_n-\gamma_m)^2}$) is generally not the shortest angular path between two junctions. Rather, the shortest path is given by the single-axis rotation about an arbitrary unit vector that transforms one helix into the other. Thus, the ‘distance’ separating two interhelical junctions, n and m, in Euler space does not provide an accurate measure of the orientation similarity between the two interhelical junctions and will generally overestimate the real differences. The difference in the orientation in two junctions n and m can be rigorously quantified by computing the amplitude, θ_{nm}, of the single-axis rotation that transforms H2(n) into H2(m) following superposition of H1 (refs. 50, 51). The relevant rotation, R_{nm}, which rotates H2(n) into iH2(m), can be calculated using

$$R_{nm} = R_m^{-1} \times R_n = R(-\gamma_m - \beta_m - \alpha_m) \times R(\alpha_n \beta_n \gamma_n)$$

in which R_n and R_m are the Euler rotations that define the helix orientation in junctions n and m, respectively. R_{nm} can then reparameterized in terms of a single-axis rotation, equation (3) (Table 1), where $\nu_{xyz} = (\nu_x, \nu_y, \nu_z)$ is the unit vector defining the rotation axis and θ_{nm}, is the rotation angle. Alternatively, θ_{nm} can be obtained through the relation $\cos(\theta_{nm}) = \frac{1}{2}[\mathrm{Tr}(R_{nm}) - 1]$, where R_{nm} is defined as above.

In general, the distance in Euler space will increasingly overestimate the real difference in orientation between two interhelical junctions as the helices approach near perfect parallel or antiparallel orientations. For example, the interhelical orientations (α_h, β_h, γ_h) = (10°, 10°, −10°) and (40°, 10°, −40°) differ by 42.4° in Euler space but are related by a single-axis rotation of amplitude 5.2°. By contrast, (10°, 90°, −10°) and (40°, 90°, −40°) differ in Euler space by 42.4° and by a single-axis rotation of amplitude 42.2°. It is also noteworthy that any error associated with the computation of an interhelical orientation will not propagate uniformly across the three angles. For example, larger deviations are expected for the angles α_h and γ_h when $|\beta_h| < 10°$ or $|\beta_h| > 170°$. Simulations using a total of 18 nonidealized A-form helices obtained from the PDB containing eight WC and G-U base pairs indicate that local deviations from the assumed idealized A-form helix structure leads to uncertainty in (α_h, β_h, γ_h) that is on the order of ~5°. However, as $|\beta_h|$ nears 0° or 180° different combinations of α_h and γ_h can yield very similar orientations and, correspondingly, the associated alignment error increases dramatically, sometimes to > 25° in α_h and γ_h.

Author Manuscript Author Manuscript Author Manuscript Author Manuscript

Therefore, large differences in α_h and γ_h between two junctions with near perfectly parallel or anti-parallel orientations can be misleading and should be interpreted with caution.

An alternative approach for depicting the interhelical Euler angles is to use Sanson-Flamsteed (SF) projection maps[52] (e.g., Fig. 4c). SF maps have widely been used to depict the relative orientation of chiral fragments determined with the use of NMR residual dipolar couplings[53]. In an SF map, the orientation of an object (i.e., H2′) defined by local coordinate $\dot{X}\dot{Y}\dot{Z}$ relative to a reference *(XYZ)* frame (i.e., H2) is depicted by plotting the orientation of the three $\dot{X}\dot{Y}\dot{Z}$ unit vectors on the surface of a globe. In other words, one uses the rotation R^{-1} that transforms iH2 to iH2′ to transform three unit vectors from XYZ to $\dot{X}\dot{Y}\dot{Z}$ and the latter is depicted on the globe. The SF projection maps the surface of a unit sphere into a plane by converting latitude (ϕ) and longitude (λ) to Cartesian coordinates (x,y) via $y = \phi$ and $x = \lambda\cos\phi$ The horizontal lines of latitude run from −90° to 90° in 10° increments, whereas vertical curved lines of longitude run from −180° to 180° in 20° increments. Any point in this plot represents the orientation of the local iH2′ axis (XYZ) relative to the reference coaxial iH2 (XYZ). The SF maps provide a convenient approach for visualizing the shape of the interhelical distribution devoid of some of the above-mentioned complications accompanied by 3D Euler maps. However, they are less useful in obtaining insights into how the three interhelical Euler angles covary with one another.

MATERIALS

EQUIPMENT

- Computer equipped with Perl version 5.0 or higher
- Structural data available in PDB format that have been generated by the user or obtained from the protein data bank or nucleic acid database
- Insight II or equivalent molecular builder programs, like ASSEMBLE[54] and other proprietary or open-access software
- Software to calculate helix parameters. Appropriate programs include Curves 5.1 (ref. 55), FreeHelix98 (ref. 56), 3DNA[7,57], SCHNAaP[58], NUPARM and NUCGEN[59], which can be used to compute the relevant helix parameters
- Software to superimpose structures (e.g., INSIGHT II 2000.1; Molecular Simulations and TINKER[60] (http://dasher.wustl.edu/tinker), as well as other similar packages).

PROCEDURE

Build reference A-form helix

1. Build a reference two-way junction consisting of two idealized and continuous A-form helices (iH1 and iH2) of length equal to helices 1 and 2 (H1 and H2) in a given target junction. The reference helix can be constructed with any sequence, as superpositions are done using the backbone phosphates, carbon and oxygen sugar atoms.

Author Manuscript Author Manuscript Author Manuscript Author Manuscript

! CAUTION If you are building helices using INSIGHT II 2000.1, care needs to be taken to correct the propeller twist angles to the proper value of −14.50. Programs such as Curves 5.1 (ref. 55), FreeHelix98 (ref. 56), 3DNA[7,57], SCHNAaP[58], NUPARM and NUCGEN[59] can be used to compute relevant helix parameters.

2. Rotate the reference helix so that its axis is oriented along the molecular *Z*-direction running toward the positive direction from iH1 to iH2.

! CAUTION Failure to properly orient the reference helix will lead to incorrect measurement of interhelical Euler angles. Care should be taken to ensure that this step is done correctly. You can easily determine whether the helix axis has been correctly aligned with respect to the molecular axis by determining the helical rise between subsequent phosphates, or between any set of identical atoms from neighboring base pairs, as it relates to the molecular frame (e.g., the difference in the *z*-component between sets of sequential phosphates, P_i. and P_{i+1}). For a correctly aligned helix, this *z*-component difference should be equal to the helical rise of an idealized A-form base-pair step (~2.8 Å).

Superimposing RNA helices

1. Identify WC base pairs in helices H1 and H2 of the target junction, J, to be used in measurement of interhelical Euler angles that are adjacent to other WC base pairs (Step 1 in Fig. 1).

! CAUTION Terminal base pairs and base pairs that immediately neighbor junctions or other noncanonical base pairs can significantly deviate from idealized A-form geometry and may result in unreliable superposition; exercise caution if using such base pairs. The use of > 5 base pairs may also result in inaccurate interhelical angles if there are significant helix bending or over/under-twisting deviations. The user may also choose to align with non-WC base pairs in circumstances where the non-WC base pair possesses backbone conformations highly similar to that of WC A-form helices. In all special cases, take careful note of the final superposition RMSD (Step 4).

2. Use backbone (phosphate) and sugar heavy atoms (i.e., carbon and oxygen) to superimpose identified base pairs in H1 in a target junction onto the corresponding base pairs and iH1 in the reference junction, applying the necessary translations and rotations to the entire junction, to obtain the new coordinates for the junction, J (Fig. 2).

! CAUTION RMSD superposition should be <2 Å, otherwise computed interhelical angles will be unreliable. An RMSD < 2 Å will typically yield errors in (α_h, β_h, γ_h) that are on the order of ~5°.

CRITICAL STEP Base atoms are not used in superposition to avoid potential distortions arising from sequence-directed variations in base and base-step parameters.

? TROUBLESHOOTING

Author Manuscript Author Manuscript Author Manuscript Author Manuscript

3. Superimpose a copy of iH2 onto H2′ in J using the same procedure described in Step 4. Save the coordinates of resulting iH2′ (Fig. 2).

4. Measure interhelical Euler angles using EULER-RNA (http://hashimi.biop.lsa.umich.edu/index.php?q=node/6). The program uses the coordinates of iH2 and iH2′ to compute a rotation matrix R, which rotates iH2′ into iH2 (see Fig. 3). The *R* matrix is then parameterized in terms of the three Euler angles α_h, β_h and γ_h (see Fig. 3).

   CRITICAL STEP Make sure to input iH2 and iH2′ in the correct order; otherwise, inconsistent angles will be obtained.

   ! CAUTION See section on ‘Definition of Euler Angles‘ for a rigorous definition.

   ? TROUBLESHOOTING

5. Select a single set of Euler angles from two degenerate sets by choosing the angles that minimize $\delta = \sqrt{\alpha_h^2 + \beta_h^2 + \gamma_h^2}$ (note that $-180° \leq \alpha_h, \beta_h, \gamma_h \leq 180°$).

   ! CAUTION For the special case of perfectly parallel or antiparallel helices, there is a continuous coaxial degeneracy defined by ($\alpha_h \pm D$, $\beta_h = 0°$ or 180°, $\gamma_h \mp D$), where *D* is a constant.

   ? TROUBLESHOOTING

6. Find the value of $T_h°$ that minimizes $\Sigma_i \delta_i$, when applying the filters for lifting the twofold degeneracy, where *i* represents the various junctions in a particular ensemble or collection. Update interhelical Euler angles α_h and γ_h to $\alpha_h + T_h$ and $\gamma_h - T_h$.

   CRITICAL STEP Use the same $T_h°$ value when comparing angles for a set of junctions.

Mapping and interpreting interhelical Euler angles

1. Plot selected interhelical angles using the approaches described in Figure 3 and as detailed under the section ‘Mapping and interpreting interhelical Euler angles’.

2. Measure similarity between interhelical junctions. The orientation similarity between two interhelical junctions, n and m, can be determined by computing the rotation matrix (R_{nm}), which rotates H2(n) into H2(m), as described under the section ‘Mapping and interpreting interhelical Euler angles’.

3. Compute fraction of space sampled by a set of interhelical junctions. To calculate the fraction of total (α_h, β_h, γ_h) space sampled by a set of junctions, round each (α_h, β_h, γ_h) angle into the nearest binned degree increment (e.g., 1°, 5° or 10°, etc.). As an example, the angle (−95.5°, 13.12°, −2.0°) is rounded to (−95°, 15°, 0°) for increments of 5°. Count all unique rounded α_h, β_h and γ_h angles and divide by the total unique permutations of α_h, β_h and γ_h on a grid of the same-degree increment, given the previously discussed degeneracies.

Author Manuscript Author Manuscript Author Manuscript Author Manuscript

? TROUBLESHOOTING

Troubleshooting advice can be found in Table 2.

ANTICIPATED RESULTS

The computed interhelical angles for a given junction are expected to fall within a relatively narrow range of conformations that are allowed based on simple steric and connectivity constraints—collectively referred to as 'topological constraints'[10,42]. In Figure 5, we use 3D maps to show the interhelical angles computed for a variety of RNA junctions from the PDB (in color) along with the computed topologically allowed space (in gray). Note that the accessible conformations will vary with the junction topology. For example, the accessible interhelical angles for bulge junctions gradually increase from 4% to 14% in going one to three nucleotide bulges (gray angles, Fig. 5). Note also the existence of correlations between the angles α_h and γ_h, which increase with the shortening of the bulge length (Fig. 5). These correlations are evident even when considering junctions with $\beta_h > 10°$ and arise naturally due to the topology of nucleic-acid two-way junctions. The allowed space also varies with the asymmetry of the junction[42]. In particular, a survey of the PDB reveals that residues within two-way junction have a high propensity to loop inside and maximize the number of pseudo-base pairs[42]. With this assumption, one expects a systematic interhelical over-twisting, resulting in an increase of $\alpha_h + \gamma_h$ by $Y \times \sim(-34°)$, in which Y corresponds to the number of residues in the shorter junction single strand (Fig. 5). Note that deviations from maximum pseudo-base-pairing states can arise[42].

We have made the set of topologically allowed angles calculated on a five-degree grid for S_1S_0, S_2S_0, S_3S_0, S_4S_0, S_1S_1, S_2S_1, S_3S_1, S_4S_1, S_2S_2, S_3S_2 S_4S_2, S_3 S_3, $S_4.S_3$, and S_4,S_4, junction motifs with T_h. = 51.1°, which is available for download in .txt file format at http://hashimi.biop.lsa.umich.edu/index.php?q=node/6. With the applicable topologically allowed space, you can measure the extent to which a set of angles falls within this space. Here you can iterate through the list of allowed angles and compute the Euclidean distance $d = \sqrt{(\alpha_{A,i} - \alpha_h)^2 + (\beta_{A,i} - \beta_h)^2 + (\gamma_{A,i} - \gamma_h)^2}$, where ($\alpha_h$, β_h, γ_h) is the angle of interest and ($\alpha_{A,i}$, $\beta_{A,i}$, $\gamma_{A,i}$) is the topologically allowed angle with index i. If the minimum distance over all topologically allowed angles is ≤10° then the conformation is allowed. The large majority of two-way junctions should fall within this allowed space. Note that for this comparison to be effective, the angle must have been computed using a reference helix with the same T_h° as that of the nature_frmhlx.pdb helix used to compute the space, as provided at http://hashimi.biop.lsa.umich.edu/index.php?q=node/6. Otherwise, as discussed above, the measured angle and its corresponding angle within the topologically allowed space will be off by ($\alpha_h \pm T_h$°, β_h = 0° or 180°, $\gamma_h \mp T_h$°).

ACKNOWLEDGMENTS

We thank D. Herschlag and V. Chu of Stanford University for stimulating discussions. A.M.M. acknowledges support from a Graduate Research Fellowship from the National Science Foundation (NSF). H.M.A.-H. acknowledges support from a NSF CAREER award (MCB 0644278) and a National Institutes of Health grant (R01GM089846). C.L.B. acknowledges funding for the Center for Multi-scale Modeling Tools for Structural Biology by the National Center for Research Resources (P41RR012255).

Author Manuscript Author Manuscript Author Manuscript Author Manuscript

References

1. Hooft RW, Sander C & Vriend G Objectively judging the quality of a protein structure from a Ramachandran plot. Comput. Appl. Biosci 13, 425–430 (1997). [PubMed: 9283757]
2. Bertini I, Cavallaro G, Luchinat C & Poli I A use of Ramachandran potentials in protein solution structure determinations. J. Biomol. NMR 26, 355–366 (2003). [PubMed: 12815262]
3. Gopalakrishnan K, Sheik SS, Ranjani CV, Udayakumar A & Seka K Conformational Angles DataBase (CADB-3.0). Prot. Pept. Lett 14, 665–668 (2007).
4. Wu D, Jernigan R & Wu Z Refinement of NMR-determined protein structures with database derived mean-force potentials. Proteins 68, 232–242 (2007). [PubMed: 17387736]
5. Kumar MV & Swaminathan R A novel approach to segregate and identify functional loop regions in protein structures using their Ramachandran maps. Proteins 78, 900–916 (2010). [PubMed: 19899172]
6. MacDonald JT, Maksimiak K, Sadowski MI & Taylor WR *De novo* backbone scaffolds for protein design. Proteins 78, 1311–1325 (2010). [PubMed: 20017215]
7. Olson WK et al. A standard reference frame for the description of nucleic acid base-pair geometry. J. Mol. Biol 313, 229–237 (2001). [PubMed: 11601858]
8. Neidle S Oxford Handbook of Nucleic Acid Structure (Oxford University Press, 1999).
9. Duarte CM & Pyle AM Stepping through an RNA structure: a novel approach to conformational analysis. J. Mol. Biol 284, 1465–1478 (1998). [PubMed: 9878364]
10. Chu VB et al. Do conformational biases of simple helical junctions influence RNA folding stability and specificity? RNA 15, 2195–2205 (2009). [PubMed: 19850914]
11. Koch MH, Vachette P & Svergun DI Small-angle scattering: a view on the properties, structures and structural changes of biological macromolecules in solution. Q. Rev. Biophys 36, 147–227 (2003). [PubMed: 14686102]
12. Patkowski A, Eimer W & Dorfmüller T Internal dynamics of tRNA(Phe) studied by depolarized dynamic light scattering. Biopolymers 30, 975–983 (1990). [PubMed: 2092826]
13. Anunciado D et al. Characterization of the dynamics of an essential helix in the U1A protein by time-resolved fluorescence measurements. J. Phys. Chem. B 112, 6122–6130 (2008). [PubMed: 18293956]
14. Cherny DI, Eperon IC & Bagshaw CR Probing complexes with single fluorophores: factors contributing to dispersion of FRET in DNA/RNA duplexes. Eur. Biophys. J 38, 395–405 (2009). [PubMed: 19015840]
15. Leontis NB & Westhof E Geometric nomenclature and classification of RNA base pairs. RNA 7, 499–512 (2001). [PubMed: 11345429]
16. Bhattacharyya A, Murchie A & Lilley DM RNA bulges and the helical periodicity of double-stranded RNA. Nature 343, 484–487 (1990). [PubMed: 2300191]
17. Lilley DM Folding of branched RNA species. Biopolymers 48, 101–112 (1998). [PubMed: 11180044]
18. Goody TA, Lilley DM & Norman DG The chirality of a four-way helical junction in RNA. J. Am. Chem. Soc 126, 4126–4127 (2004). [PubMed: 15053600]
19. Musselman C et al. Impact of static and dynamic A-form heterogeneity on the determination of RNA global structural dynamics using NMR residual dipolar couplings. J. Biomol. NMR 36, 235–249 (2006). [PubMed: 17077936]
20. Gast FU, Amiri KM & Hagerman PJ. Interhelix geometry of stems I and II of a self-cleaving hammerhead RNA. Biochemistry 33, 1788–1796 (1994). [PubMed: 7509191]
21. Leehey MA, Squassoni CA, Friederich MW, Mills JB & Hagerman PJ A noncanonical tertiary conformation of a human mitochondrial transfer RNA. Biochemistry 34, 16235–16239 (1995). [PubMed: 8845346]
22. Zacharias M & Hagerman PJ. Bulge-induced bends in RNA: quantification by transient electric birefringence. J. Mol. Biol 247, 486–500 (1995). [PubMed: 7536250]
23. Zacharias M & Hagerman PJ. The influence of symmetric internal loops on the flexibility of RNA. J. Mol. Biol 257, 276–289 (1996). [PubMed: 8609623]

Author Manuscript Author Manuscript Author Manuscript Author Manuscript

24. Zacharias M & Hagerman PJ. Influence of static and dynamic bends on the birefringence decay profile of RNA helices: Brownian dynamics simulations. Biophys. J 73, 318–332 (1997). [PubMed: 9199796]
25. Nakamura TM, Wang YH, Zaug AJ, Griffith JD & Cech TR Relative orientation of RNA helices in a group 1 ribozyme determined by helix extension electron microscopy. EMBO J. 14, 4849 (1995). [PubMed: 7588614]
26. Amiri KMA & Hagerman PJ. Global conformation of a self-cleaving hammerhead RNA. Biochemistry 33, 13172–13177 (1994). [PubMed: 7947724]
27. Al-Hashimi HM et al. Concerted motions in HIV-1 TAR RNA may allow access to bound state conformations: RNA dynamics from NMR residual dipolar couplings. J. Mol. Biol 315, 95–102 (2002). [PubMed: 11779230]
28. Zhang Q, Sun X, Watt ED & Al-Hashimi HM Resolving the motional modes that code for RNA adaptation. Science 311, 653–656 (2006). [PubMed: 16456078]
29. Hansen AL & Al-Hashimi HM Dynamics of large elongated RNA by NMR carbon relaxation. J. Am. Chem. Soc 129, 16072–16082 (2007). [PubMed: 18047338]
30. Zhang Q, Stelzer AC, Fisher CK & Al-Hashimi HM Visualizing spatially correlated dynamics that directs RNA conformational transitions. Nature 450, 1263–1267 (2007). [PubMed: 18097416]
31. Getz MM, Andrews AJ, Fierke CA & Al-Hashimi HM Structural plasticity and Mg2+ binding properties of RNase P P4 from combined analysis of NMR residual dipolar couplings and motionally decoupled spin relaxation. RNA 13, 251–266 (2007). [PubMed: 17194721]
32. Zhang Q & Al-Hashimi HM Extending the NMR spatial resolution limit for RNA by motional couplings. Nat. Methods 5, 243–245 (2008). [PubMed: 18246076]
33. Hansen AL, Nikolova EN, Casiano-Negroni A & Al-Hashimi HM Extending the range of microsecond-to-millisecond chemical exchange detected in labeled and unlabeled nucleic acids by selective carbon R(1rho) NMR spectroscopy. J. Am. Chem. Soc 131, 3818–3819 (2009). [PubMed: 19243182]
34. Zhang Q & Al-Hashimi HM Domain-elongation NMR spectroscopy yields new insights into RNA dynamics and adaptive recognition. RNA 15, 1941–1948 (2009). [PubMed: 19776156]
35. Dethoff EA, Hansen AL, Zhang Q & Al-Hashimi HM Variable helix elongation as a tool to modulate RNA alignment and motional couplings. J. Magn. Reson 202, 117–121 (2010). [PubMed: 19854083]
36. Bax A & Grishaev A Weak alignment NMR: a hawk-eyed view of biomolecular structure. Curr. Opin. Struct. Biol 15, 563–570 (2005). [PubMed: 16140525]
37. Lipsitz RS & Tjandra N Residual dipolar couplings in NMR structure analysis. Annu. Rev. Biophys. Biomol. Struct 33, 387–413 (2004). [PubMed: 15139819]
38. MacDonald D & Lu P Residual dipolar couplings in nucleic acid structure determination. Curr. Opin. Struct. Biol 12, 337–343 (2002). [PubMed: 12127452]
39. Casiano-Negroni A, Sun X & Al-Hashimi HM Probing Na(+)-induced changes in the HIV-1 TAR conformational dynamics using NMR residual dipolar couplings: new insights into the role of counterions and electrostatic interactions in adaptive recognition. Biochemistry 46, 6525–6535 (2007). [PubMed: 17488097]
40. Getz M, Sun X, Casiano-Negroni A, Zhang Q & Al-Hashimi HM NMR studies of RNA dynamics and structural plasticity using NMR residual dipolar couplings. Biopolymers 86, 384–402 (2007). [PubMed: 17594140]
41. Bailor MH et al. Characterizing the relative orientation and dynamics of RNA A-form helices using NMR residual dipolar couplings. Nat. Protoc 2, 1536–1546 (2007). [PubMed: 17571061]
42. Bailor MH, Sun X & Al-Hashimi HM Topology links RNA secondary structure with global conformation, dynamics, and adaptation. Science 327, 202–206 (2010). [PubMed: 20056889]
43. Gelbin A et al. Geometric parameters in nucleic acids: sugar and phosphate constituents. J. Am. Chem. Soc 118, 519–529 (1996).
44. Nelson JW, Martin FH & Tinoco I DNA and RNA oligomer thermodynamics: the effect of mismatched bases on double-helix stability. Biopolymers 20, 2509–2531 (1981). [PubMed: 7326358]

Author Manuscript Author Manuscript Author Manuscript Author Manuscript

45. Holbrook SR & Kim SH Local mobility of nucleic acids as determined from crystallographic data. I. RNA and B form DNA. J. Mol. Biol 173, 361–388 (1984). [PubMed: 6199506]
46. Foloppe N & MacKerell AD Jr. Conformational properties of the deoxyribose and ribose moieties of nucleic acids: a quantum mechanical study. J. Phys. Chem. B 102, 6669–6678 (1998).
47. Lilley DM et al. A nomenclature of junctions and branchpoints in nucleic acids. Nucleic Acids Res. 23, 3363–3364 (1995). [PubMed: 16617514]
48. Yang H et al. Tools for the automatic identification and classification of RNA base pairs. Nucleic Acids Res. 31, 3450–3460 (2003). [PubMed: 12824344]
49. Varshalovich DA, Moskalev AN & Khersonskii VK Quantum Theory of Angular Momentum (World Scientific Pub. Co., 1987).
50. Tolman JR, Al-Hashimi HM, Kay LE & Prestegard JH Structural and dynamic analysis of residual dipolar coupling data for proteins. J. Am. Chem. Soc 123, 1416–1424 (2001). [PubMed: 11456715]
51. Fisher CK & Al-Hashimi HM Approximate reconstruction of continuous spatially complex domain motions by multialignment NMR residual dipolar couplings. J. Phys. Chem. B 113, 6173–6176 (2009). [PubMed: 19358547]
52. Bugayevskiy LM & Snyder JP Map Projections: A Reference Manual (Blackwell Publishers, 1996).
53. Losonczi JA, Andrec M, Fischer MWF & Prestegard JH Order matrix analysis of residual dipolar couplings using singular value decomposition. J. Mag. Reson 138, 334–342 (1999).
54. Jossinet F, Ludwig TE & Westhof E Assemble: an interactive graphical tool to analyze and build RNA architectures at the 2D and 3D levels. Bioinformatics 26, 2057–2059 (2010). [PubMed: 20562414]
55. Ravishanker G, Swaminathan S, Beveridge DL, Lavery R & Sklenar H Conformational and helicoidal analysis of 30 PS of molecular dynamics on the d (CGCGAATTCGCG) double helix: ‘curves’, dials and windows. J. Biomol. Struct. Dyn 6, 669–699 (1989). [PubMed: 2619934]
56. Dickerson RE DNA bending: the prevalence of kinkiness and the virtues of normality. Nucleic Acids Res. 26, 1906–1926 (1998). [PubMed: 9518483]
57. Lu XJ & Olson WK 3DNA: a software package for the analysis, rebuilding and visualization of three-dimensional nucleic acid structures. Nucleic Acids Res. 31, 5108–5121 (2003). [PubMed: 12930962]
58. Lu XJ, El Hassan MA & Hunter CA Structure and conformation of helical nucleic acids: analysis program (SCHNAaP). J. Mol. Biol 273, 668–680 (1997). [PubMed: 9356255]
59. Bansal M, Bhattacharyya D & Ravi B NUPARM and NUCGEN: software for analysis and generation of sequence dependent nucleic acid structures. Comput. Appl. Biosci 11, 281–287 (1995). [PubMed: 7583696]
60. Ren P & Ponder JW Consistent treatment of inter- and intramolecular polarization in molecular mechanics calculations. J. Comput. Chem 23, 1497–1506 (2002). [PubMed: 12395419]

Author Manuscript Author Manuscript Author Manuscript Author Manuscript

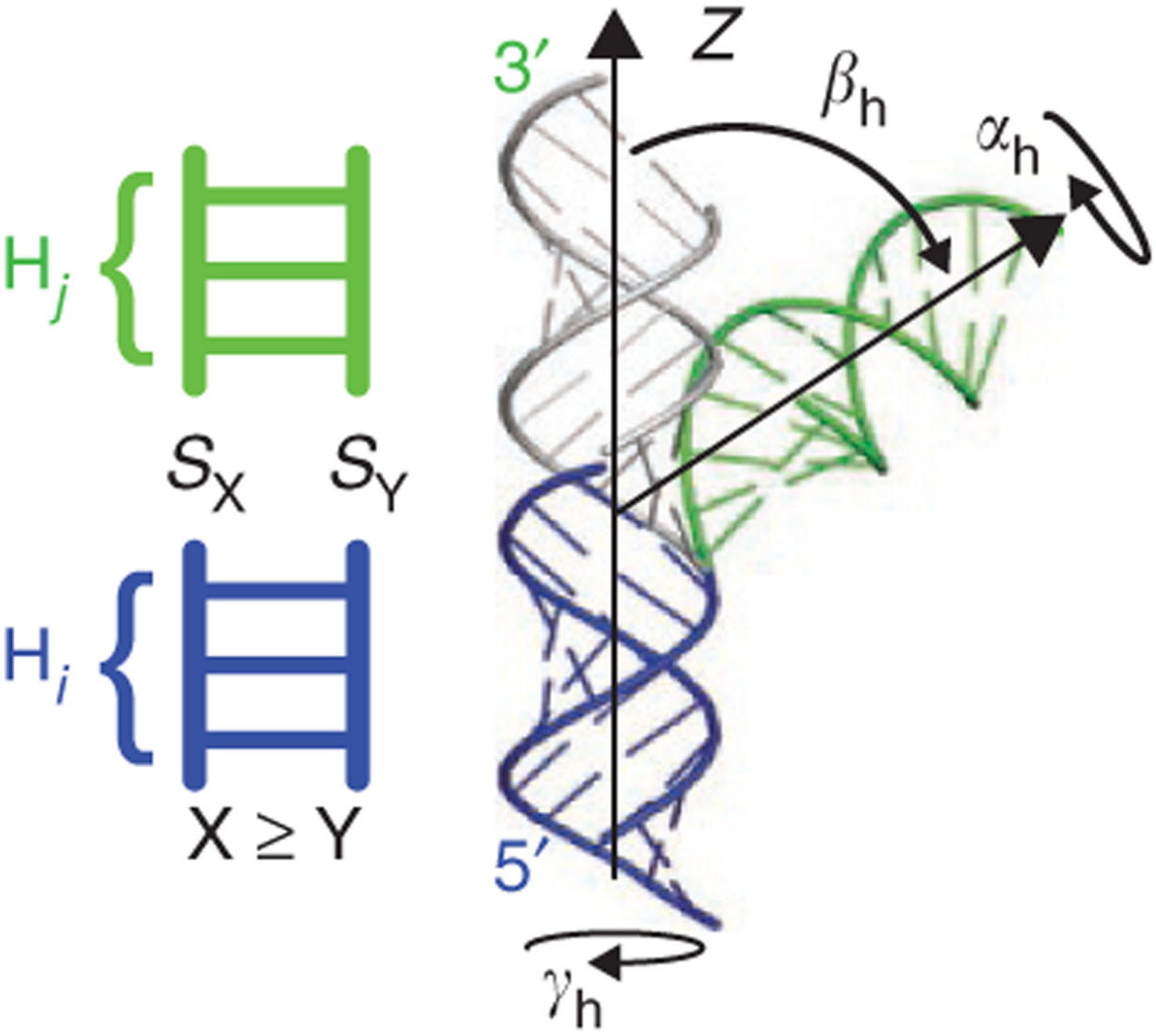

Figure 1 |.

Interhelical Euler angles. Angles (α_h, β_h, γ_h) specify the orientation of 5′ and 3′ helices (H_i and H_j) across two-way junctions with i and j number of base pairs, respectively, and topology defined by the length of two junction strands (S_X and S_Y) for idealized helices whose helical axes are oriented coaxial to the molecular z axis.

Author Manuscript Author Manuscript Author Manuscript Author Manuscript

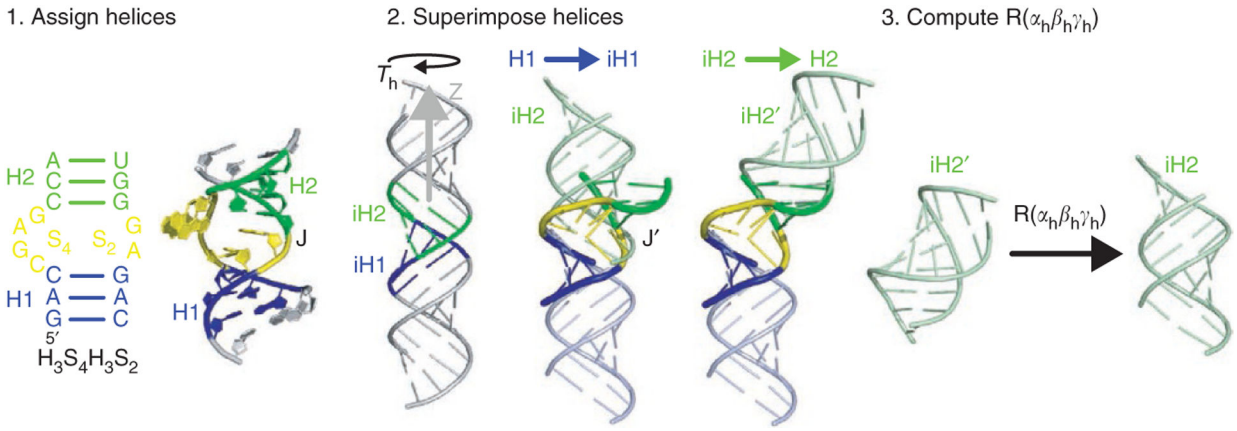

Figure 2 |.

General scheme for computing interhelical Euler angles. (1) helices within a target junction (H1 and H2 shown in blue and green, respectively) that is adjacent to a two-way junction (yellow) are identified and assigned. Reference idealized A-form helices (iH1 and iH2 shown in blue and green, respectively) are constructed and oriented along the molecular *Z* direction. (2) Superposition of H1 transforms J into the reference frame of iH1. A following superposition places iH2 into the observed orientation of H2. (3) The interhelical Euler angles are calculated using EULER-RNA, and represent the transformation of iH2′ back to its original orientation (iH 2).

Author Manuscript Author Manuscript Author Manuscript Author Manuscript

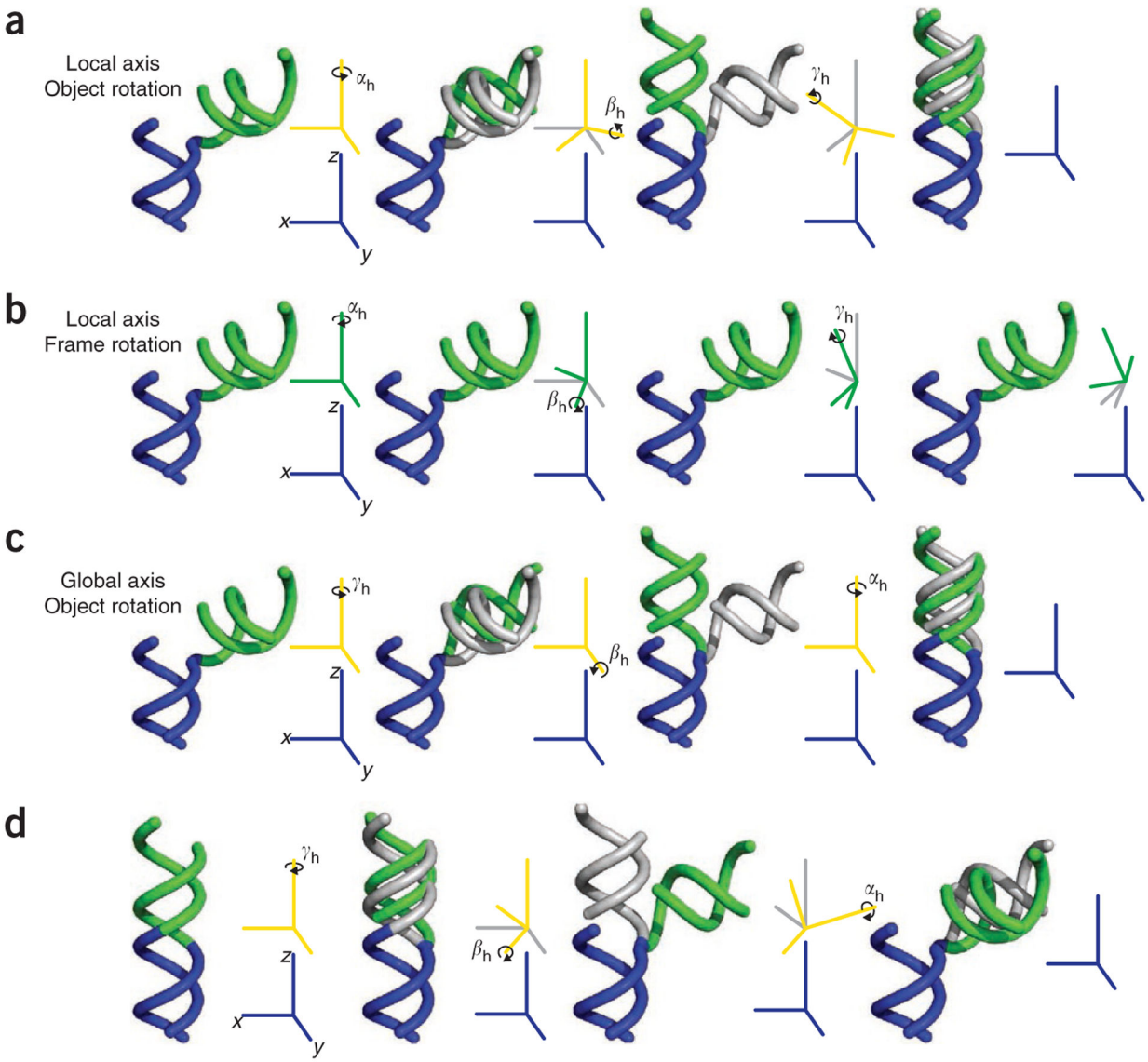

Figure 3 |.

Definition of Euler rotation matrix and angles. (**a–c**) The Euler rotation matrix and angles can be conceptualized as: object rotation around a local axis (**a**), frame rotation around a local axis (**b**), or object rotation around a global axis (**c**). (**d**) The inverse rotation can be used to generate an interhelical structure and provides an intuitive description of the Euler angles. Note that different rotations (clockwise versus anticlockwise) are applied in different cases.

Author Manuscript Author Manuscript Author Manuscript Author Manuscript

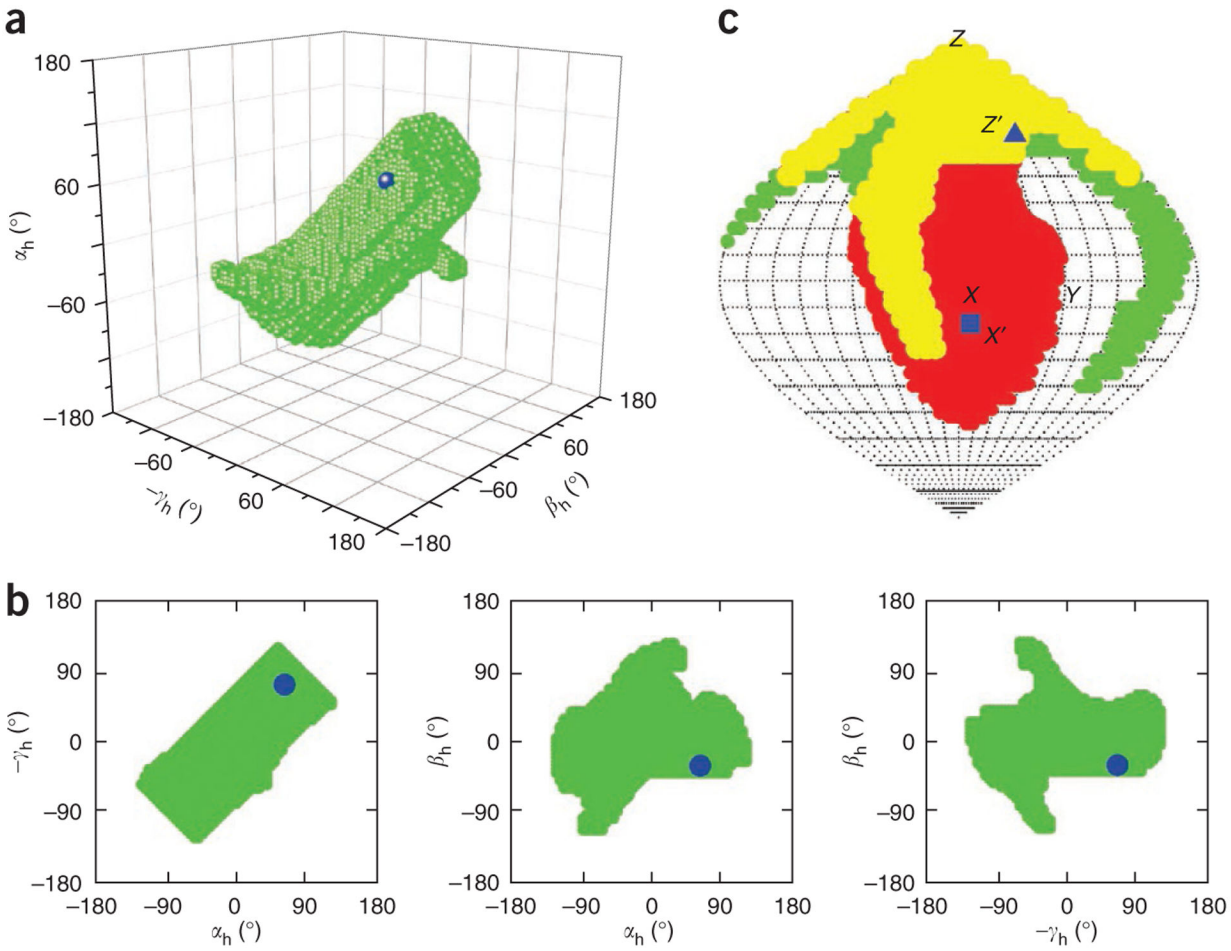

Figure 4 |.

Approaches for mapping interhelical Euler angles. (**a–c**) 3D map (**a**), three 2D maps (**b**) and Sanson-Flamsteed (SF) projection maps (**c**). A single RNA conformation is highlighted by a blue sphere and circle in Euler space (**a**,**b**) and the triangle and square in SF projection maps (**c**). The green spheres and circles in the Euler space (**a**,**b**) represent the topologically available space for an S_2S_0 RNA junction. In the SF projection (**c**), red, green, and yellow circles represent the topologically available space for the *x, z,* and overlaps between the *x* and *z* axes, respectively. The molecular *y* axis is marked as a reference, although the allowed space for the y axis has been excluded for clarity.

Author Manuscript Author Manuscript Author Manuscript Author Manuscript

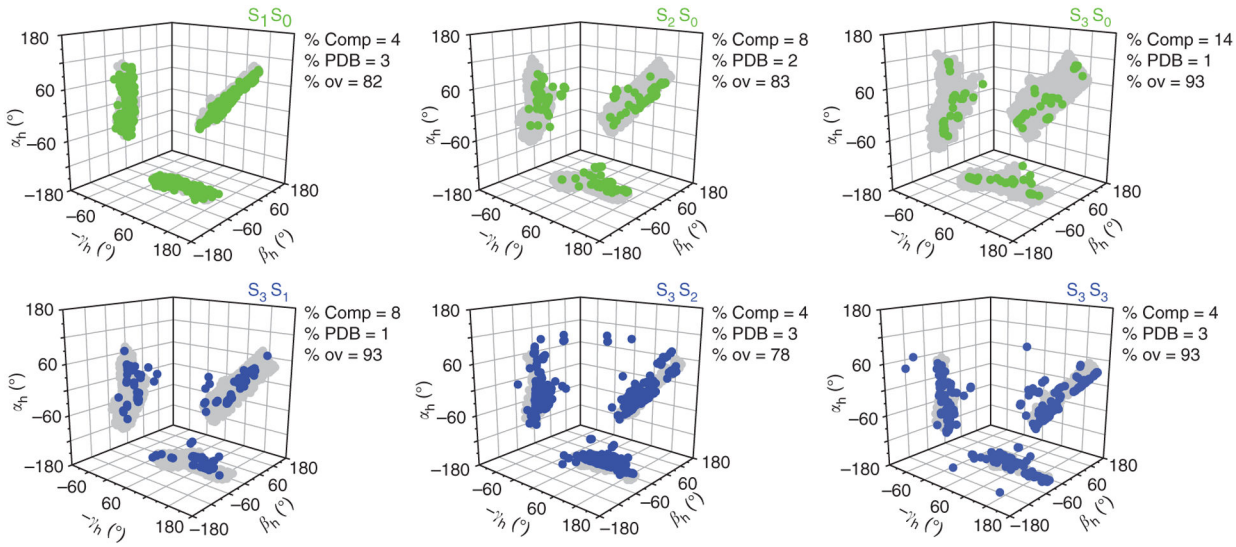

Figure 5 |.

Topological confinement and distribution of RNA interhelical orientations; 3D interhelical orientation maps showing the individual 2D projections along each plane. The PDB-derived (gray) and topologically computed interhelical distributions for different types of bulges (green) and internal loops (blue) are shown. Increasing junction length of the *X* strand leads to increased breadth of the conformational distribution, as shown for 1–0, 2–0 and 3–0 junctions; however, increasing *Y* strand length results in changes to the relative distribution of orientations between two helices, as shown by 3–1, 3–2 and 3–3 junctions, that shifts the ensemble of conformers within α_h-γ_h space. The percentage of interhelical orientations sampled by the PDB-derived and topologically computed distributions is indicated (Ω_{PDB} and Ω_{comp}, respectively) along with the fraction of the PDB-derived orientations that falls within 10° of the topologically allowed distribution (Ω_{ov}).

Author Manuscript Author Manuscript Author Manuscript Author Manuscript

TABLE 1 |

Equations involved in the calculation and analysis of interhelical Euler angles.

	Equation
1	$$(\alpha'_{\mathrm{h}}, \beta'_{\mathrm{h}}, \gamma'_{\mathrm{h}}) = \left(-\arctan\left(\frac{\sin(\gamma_{\mathrm{h}}) + \cos(\gamma_{\mathrm{h}})\tan(2\alpha_F(T^{\circ}_{\mathrm{h}}))}{-\cos(\gamma_{\mathrm{h}}) + \sin(\gamma_{\mathrm{h}})\tan(2\alpha_F(T^{\circ}_{\mathrm{h}}))}\right),\ -\beta_{\mathrm{h}},\ -\arctan\left(\frac{-\sin(\alpha_{\mathrm{h}}) + \cos(\alpha_{\mathrm{h}})\tan(2\alpha_F(T^{\circ}_{\mathrm{h}}))}{\cos(\alpha_{\mathrm{h}}) + \sin(\alpha_{\mathrm{h}})\tan(2\alpha_F(T^{\circ}_{\mathrm{h}}))}\right)\right)$$
2	$$R(\alpha_{\mathrm{h}}\beta_{\mathrm{h}}\gamma_{\mathrm{h}}) = \begin{bmatrix} -\sin(\alpha_{\mathrm{h}})\sin(\gamma_{\mathrm{h}}) + \cos(\alpha_{\mathrm{h}})\cos(\beta_{\mathrm{h}})\cos(\gamma_{\mathrm{h}}) & -\sin(\alpha_{\mathrm{h}})\cos(\gamma_{\mathrm{h}}) - \cos(\alpha_{\mathrm{h}})\cos(\beta_{\mathrm{h}})\sin(\gamma_{\mathrm{h}}) & \cos(\alpha_{\mathrm{h}})\sin(\beta_{\mathrm{h}}) \\ \cos(\alpha_{\mathrm{h}})\sin(\gamma_{\mathrm{h}}) + \sin(\alpha_{\mathrm{h}})\cos(\beta_{\mathrm{h}})\cos(\gamma_{\mathrm{h}}) & \cos(\alpha_{\mathrm{h}})\cos(\gamma_{\mathrm{h}}) - \sin(\alpha_{\mathrm{h}})\cos(\beta_{\mathrm{h}})\sin(\gamma_{\mathrm{h}}) & \sin(\alpha_{\mathrm{h}})\sin(\beta_{h}) \\ -\cos(\gamma_{h})\sin(\beta_{h}) & \sin(\gamma_{\mathrm{h}})\sin(\beta_{\mathrm{h}}) & \cos(\beta_{\mathrm{h}}) \end{bmatrix}$$
3	$$R\left(\theta_{\mathrm{nm}}, v_{x,y,z}\right) = \begin{bmatrix} 1 + (1 - \cos\theta_{\mathrm{nm}})(v_x v_x - 1) & -v_z\sin\theta_{\mathrm{nm}} + (1 - \cos\theta_{\mathrm{nm}})v_x v_y & v_y\sin\theta_{\mathrm{nm}} + (1 - \cos\theta_{\mathrm{nm}})v_x v_z \\ v_z\sin\theta_{\mathrm{nm}} + (1 - \cos\theta_{\mathrm{nm}})v_x v_y & 1 + (1 - \cos\theta_{\mathrm{nm}})\left(v_y v_y - 1\right) & -v_x\sin\theta_{\mathrm{nm}} + (1 - \cos\theta_{\mathrm{nm}})v_y v_z \\ -v_y\sin\theta_{\mathrm{nm}} + (1 - \cos\theta_{\mathrm{nm}})v_x v_z & v_x\sin\theta_{\mathrm{nm}} + (1 - \cos\theta_{\mathrm{nm}})v_y v_z & 1 + (1 - \cos\theta_{\mathrm{nm}})(v_z v_z - 1) \end{bmatrix}$$

Nat Protoc. Author manuscript; available in PMC 2020 December 15.

Author Manuscript Author Manuscript Author Manuscript Author Manuscript

TABLE 2 |

Troubleshooting table.

Step	Problem	Possible reason	Solution
4,6	High RMSD from superimposing helices	Selection of non-Watson-Crick base-pair residues	Visually inspect superpositions of helices to ensure the correct residues have been selected; correct input residue selection of Watson-Crick base pairs as needed
	High RMSD from Superimposing helices	Mismatch of PDB file formats	If visual inspection of superposition looks to be systematically off, then the formatting among PDB files may be different causing the program to attempt fitting of helices with mismatched atoms. Change format of PDB files
	High RMSD from Superimposing helices	Incorrect number of PDB residue	Check the PDB file for the structure and reference helices for numbering of residues. Note inconsistencies and gaps in numbering. Change PDB file or input as necessary so as to select correct residues
	Poor or failed superposition of helices	Superposition algorithm	In some instances, the algorithm for the program implementing the superimposition of two helices produces incorrect results. For instance, the ‘align’ algorithm implemented in PyMol is not sufficient for properly superimposing two helices and should not be used. Instead, another algorithm or another program should be used
	Poor or failed superposition of helices	Structural deviations from A-form helix	Visually inspect superpositions of reference and structure. Often in the case of poor helix superposition, regions of disordered or non A-form atomic coordinates within the selected Watson-Crick base pairs will cause poor fitting of ideal A-form base pairs. If necessary, these atoms can be omitted from superposition, as long as you use a variety of other atoms across multiple base pairs spanning both strands in the fitting process
	Poor or failed superposition of helices	Mutations/omissions to atomic coordinates	In certain instances, heteroatoms of nucleotide analogs are included in the PDB file. Superposition of these atoms can be used in the fitting process as long as they correspond to A-form parameters. In most cases, you will need to change the atom label within the PDB file in order to carry out superposition of helices
7	Unrealistic or incorrect interhelical Euler angles	Poor superposition—see troubleshooting of step(s) 4/6	Calculation of unrealistic interhelical Euler angles is often the cause of poor superposition. One should always take care to visually inspect the superposition with the interhelical Euler angles in mind as a first step in making sure that the measured values make physical sense
	Unrealistic or incorrect interhelical Euler angles	Improper orientation of reference helix	Ensure that during the fitting procedure the reference helix is oriented in a coaxial manner to the molecular frame, and that at no time during the superposition process is it translated or rotated in anyway
	Unrealistic or incorrect interhelical Euler angles	Incorrect entry of PDB files in program EULER-RNA	One quick method to check whether the PDB files have been entered correctly in EULER-RNA is to check the sign of the helical twist (ζ). Over- and undertwisting correspond to negative and positive values, respectively, and this physical feature of the RNA can usually be visually confirmed

Nat Protoc. Author manuscript; available in PMC 2020 December 15.